JOURNAL OF SOLID STATE CHEMISTRY 69, 81–92 (1987)

Electron Microscopic Study on the Structure of an Intermediate Phase with the Composition of $BaNiO_x$ ($2 < x < 3$)

H. SHIBAHARA

Department of Chemistry, Kyoto University of Education, Fushimi-ku, Kyoto 612, Japan

Received June 30, 1986; in revised form October 17, 1986

Structures of barium–nickel oxides represented by the formulae $BaNiO_3$ and $BaNiO_2$ were studied by high-resolution electron microscopy. A new phase of $BaNiO_x$ ($2 < x < 3$) as an intermediate was also observed. From the electron diffraction patterns and high-resolution electron microscope images of an intermediate phase, topotaxial phase relations between $BaNiO_3$ and $BaNiO_2$ were deduced as follows: $[001]_{BaNiO_3}/[001]_{BaNiO_2}$ and $[100]_{BaNiO_3}/[1\bar{1}0]_{BaNiO_2}$. By *in situ* observation of phase transformation of $BaNiO_3$ with beam irradiation in electron microscopy, the formation of an intermediate phase of $BaNiO_x$ having a superstructure could be confirmed through a series of high-resolution electron microscopic images. The new phase of $BaNiO_x$ was found to have an orthorhombic unit cell represented by a superstructure of $BaNiO_2$ with $a_0 = 3a$, $b_0 = b$, $c_0 = 2c$ or of $BaNiO_3$ with $a_0 = 3a$, $c_0 = 2c$ with the composition ranging between $BaNiO_{2.33}$ and $BaNiO_{2.67}$.

Introduction

$BaNiO_3$ is a hexagonal structure with the unit cell of $a = 0.558$ and $c = 0.483$ nm closely related to that of perovskite and based on a stacking of BaO_3 layers with Ni occupying interlayer octahedral sites. The same stacking of BaO_3 as that of $BaNiO_3$ is found in a 2H (H = hexagonal) phase of $BaMnO_3$ (*1, 2*). The structure of $BaNiO_2$ is also pseudohexagonal with barium ions in a hexagonal close-packed arrangement. In $BaNiO_2$ four oxygen ions are assigned to a planar and very nearly square arrangement around nickel ions, and barium ions are surrounded by eight oxygen ions. The unit cell is orthorhombic with $a = 0.573$, $b = 0.920$, and $c = 0.473$ nm. J. J. Lander *et al.* (*3–5*) and H. Krischner *et al.* (*6*) reported the preparation and properties of barium–nickel oxide systems largely by means of X-ray diffraction. The structure type of such material has been discussed by R. D. Burbank and H. T. Evans (*7*). The perovskites with the general formula XYO_3 have been extensively studied because of their interesting ferroelectric and magnetic properties. Several authors have studied the structural modifications in the oxides of XYO_3 by means of X-ray diffraction as follows: $BaMnO_{3-x}$ and $SrMnO_{3-x}$ (*1, 2, 8, 9*), $BaRu_{1-x}M_xO_3$ (M = metal) (*10*), and $Ba_{1-x}Sr_xRuO_3$ (*11*). Detailed study of the phases in such materials by X-ray diffraction is rather difficult, because the Y cation tends to exist as a mixture of the various oxidation states. Since, however, high-resolution electron microscopy has an advantage for examining the local phase relations to each other on an atomic scale, it seems

0022-4596/87 $3.00

to be useful to use it to investigate the detailed structure of XYO_3 compounds. Thus, using electron microscope observations, the author studied the phase transformation of a 2H structure of $BaMnO_3$ into a layered structure with a long periodicity along the c-axis of the hexagonal cell (*12, 13*). In this paper the author studied the interrelation of a few phases with compositions of $BaNiO_2$, $BaNiO_3$, and $BaNiO_x$ ($2 < x < 3$) using the electron diffraction pattern and the structure image formed by high-resolution electron microscopy.

Experimental

The samples of barium–nickel oxide were prepared by the following procedure: hyperpure $BaCO_3$ and NiO were mixed in equimolar quantities for 24 hr by a magnetic stirrer. BaO was not used because of its hygroscopic property. The mixtures were treated under several conditions: (1) in vacuum at 1100°C for 6 hr followed by quenching and (2) in O_2 at 600°C for 15 hr followed by very slow cooling. The sintered products were identified by using both the X-ray powder diffraction method and the simulation of X-ray diffraction profile based on the Rietveld method (*14, 15*) in combination. X-ray powder patterns of the samples were recorded by using Ni-filtered CuK_α radiation. For electron microscopic observation, the samples were finely ground and dispersed in absolute ethanol and then mounted onto holey carbon microgrids. In order to detect the difference in structure of the sample with nonstoichiometric state, a very thin fragment was selected and its orientation was adjusted to make the incident beam direction suitable for observation by using a goniometer stage. High-resolution electron microscope images were taken with a JEM-2000EX electron microscope operated at 200 kV and direct observations of the reduction process by beam irradiation were made by removing the condenser aperture to yield a very high beam intensity when necessary. Fast Fourier transform of the high-resolution electron microscopic image was carried out to obtain the small selected area diffraction pattern.

Results and Discussion

1. $BaNiO_2$ and $BaNiO_3$

The sample held at a pressure of about 10^{-1} Pa at 1100°C for 6 hr in an electrical furnace and then cooled rapidly gave an X-ray powder diffraction pattern as shown in Fig. 1a, which agreed well with that of Ba NiO_2 phase reported by Lander (*3*). The index of Fig. 1a is based on the orthorhombic system with $a = 0.573$, $b = 0.920$, and $c = 0.473$ nm. Assuming the orthorhombic structure of $BaNiO_2$ with stoichiometric state, the calculated profile of diffraction lines using the symmetric Cauchy curve after background subtraction is illustrated in Fig. 1b. By comparing the profile of Fig. 1a with that of Fig. 1b, it could be concluded

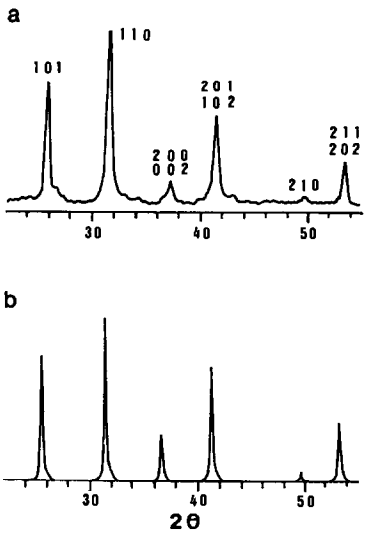

FIG. 1. (a) X-ray powder diffraction pattern of Ba NiO_2 phase with indices based on an orthorhombic structure of $BaNiO_2$ and (b) calculated relative intensities on the basis of $BaNiO_2$ with unit cell parameters of $a = 0.573$, $b = 0.920$, and $c = 0.473$ nm.

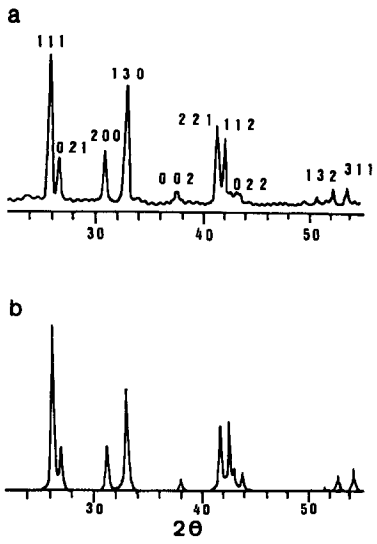

FIG. 2. (a) X-ray powder diffraction pattern of Ba NiO_3 phase with indices based on a hexagonal structure of $BaNiO_3$ and (b) calculated relative intensities on the basis of $BaNiO_3$ with unit cell parameters of a = 0.558, c = 0.483 nm.

that the sample is of an almost single Ba NiO_2 phase and this reaction carried out in vacuum at a high temperature resulted in reduction of the nickel. With prolonged heating of the sample of $BaNiO_2$ at 600°C for 15 hr in O_2 at the flow rate of about 1000 ml/min following very slow cooling to room temperature, a phase transformation took place which gave an X-ray powder diffraction pattern as shown in Fig. 2a. From the calculated profile of diffraction lines of Fig. 2b, which assumes the hexagonal structure of $BaNiO_3$ with the unit cell of a = 0.558, c = 0.483 nm, it is considered that the sample was transformed completely into $BaNiO_3$ phase by oxidation, namely, divalent nickel compounded with oxygen and barium was oxidized to the tetravalent state.

Figure 3a shows the lattice image of Ba NiO_2 phase like that in Fig. 1a by high-resolution electron microscopy, taken with an incident electron beam parallel to the [001] direction in the orthorhombic lattice. Figure 3b represents an enlargement of the region indicated by the arrow in (a) with an inset of the framework of the unit cell projected onto the (001) plane. The atomic arrangement of $BaNiO_2$ projected along the [001] direction of the orthorhombic cell is shown in Fig. 4 as reported by Lander (*3*). Figures 5a and 5b show the low magnification and enlargement of a high-resolution electron microscope image of $BaNiO_3$ phase which is identical with that of Fig. 2a. It was taken with an incident electron beam parallel to the [100] direction in the hexagonal lattice. The framework of the unit cell projected along the [100] direction is shown in the inset of Fig. 5b. Figures 6a–6i show the simulated images based on the model of 2H structure of $BaNiO_3$ by the multislice method (*16, 17*) under the following imaging conditions: the thickness of the sample was 5.6, 13.4, and 22.4 nm, f = 56, 90, and 100 nm underfocus, Cs = 1.9 mm, Cc = 1.9 mm, beam divergence angle of 1×10^{-3} rad, and accelerating voltage of 200 kV. The framework of the unit cell for simulating is represented in Fig. 6e. The simulated image in Fig. 6e is in good agreement with the observed image shown in Fig. 5b. Figure 7 shows the atomic arrangement of $BaNiO_3$ projected along the [100] direction of the hexagonal unit cell (*3*). Large solid circles in the model represent the positions of Ba atoms. It is found that the strong bright dots in the image represent the position of Ba atoms under the imaging condition of Figs. 6e and 6f.

2. $BaNiO_x$ ($2 < x < 3$)

Figure 8 shows an X-ray powder diffraction pattern of the sample which was prepared by treating the sample shown in Fig. 1a at 600°C for 6 hr in O_2 at the flow rate of about 500 ml/min following rapid cooling to room temperature. By comparing the profile of Fig. 8 with that of Fig. 1a or Fig. 2a, it is considered that the profile could be indexed hexagonally for the cell with a about

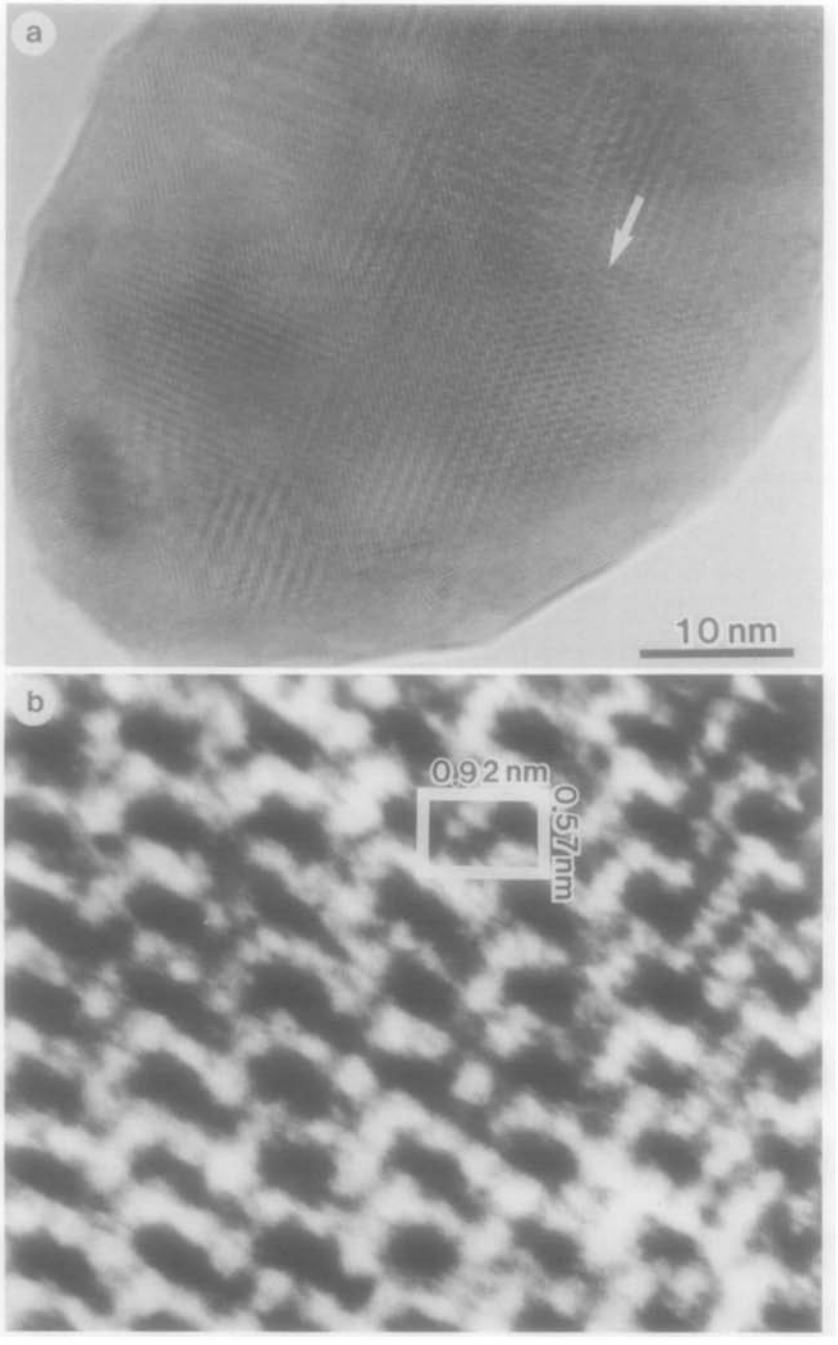

FIG. 3. (a) High-resolution electron microscope image of an orthorhombic structure in $BaNiO_2$, taken with an incident beam parallel to the [001] direction in the orthorhombic unit cell. (b) Enlargement of area near arrow with a unit cell of orthorhombic structure of $BaNiO_2$ outlined.

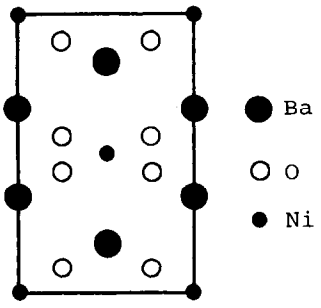

FIG. 4. Atomic arrangement of $BaNiO_2$ projected along the [001] direction of the orthorhombic cell (*3*).

0.57, c about 0.44 nm and therefore heavy atoms like Ba could have almost the same positions as those of $BaNiO_2$ or $BaNiO_3$ given above. Namely, the gross structure of the present sample resembles those of Ba NiO_2 and $BaNiO_3$. It could be interpreted as an intermediate phase with the composition of $BaNiO_x$ ($2 < x < 3$). Lander (*3*) found the intermediate of the hexagonal phase with composition near $Ba_3Ni_3O_8$ by the X-ray diffraction method. But some lattice spacings and relative intensities from the present measurement are not in agreement with those of $Ba_3Ni_3O_8$, although it has a similar unit cell size. The measured lattice spacings from the pattern of Fig. 8 are listed in Table I. For reference the data reported by Lander (*3*) for $Ba_3Ni_3O_8$ phase are included in the table. Figure 9a shows an electron microscope image of the sample with a needlelike shape. Figures 9b, 9c, and 9d show the selected area diffraction pat-

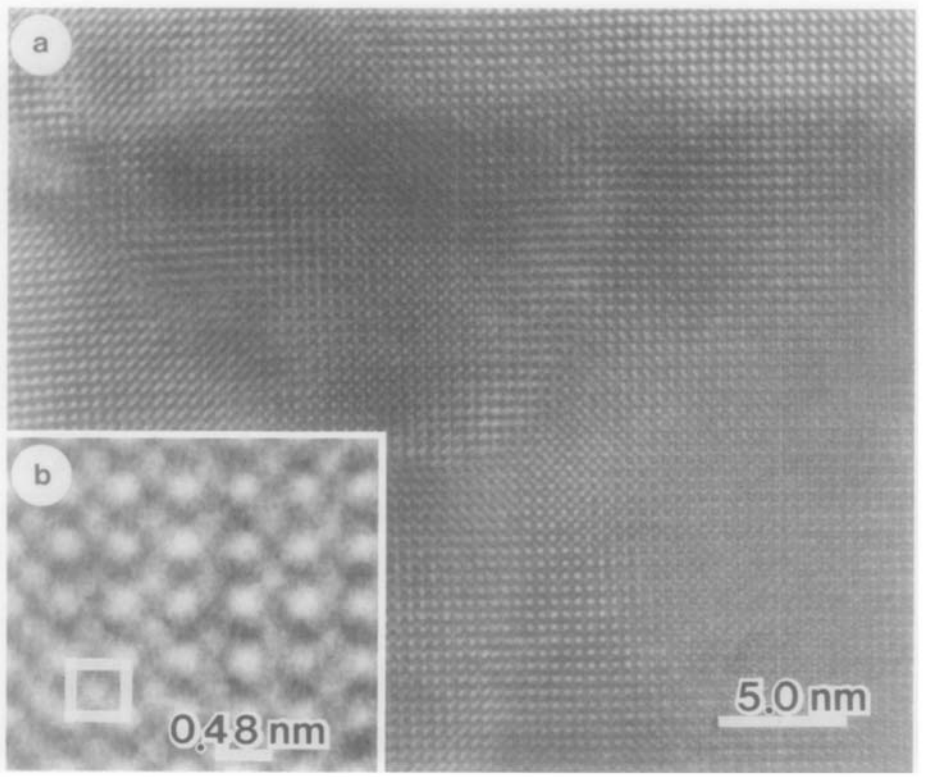

FIG. 5. (a) High-resolution electron microscope image of hexagonal structure in $BaNiO_3$, taken with an incident beam parallel to the [100] direction in the hexagonal unit cell. (b) A framework of unit cell in the hexagonal structure of $BaNiO_3$ is outlined in the enlargement.

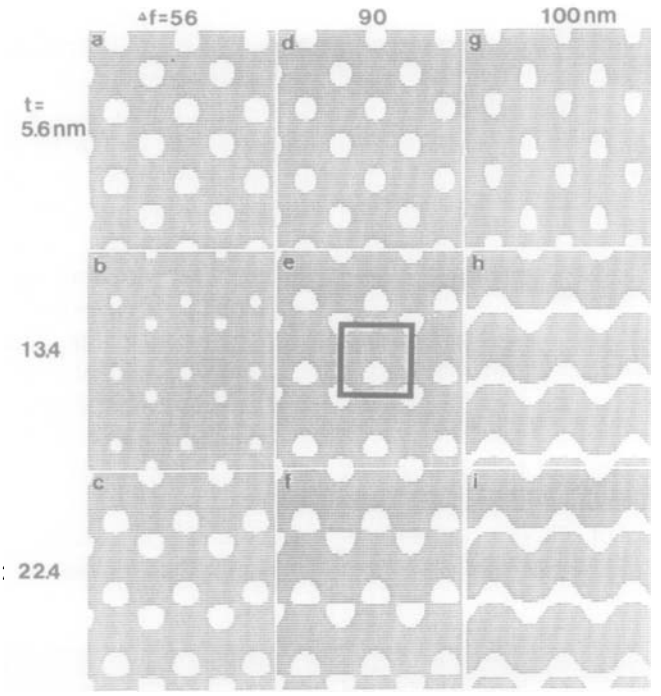

FIG. 6. Simulated images of hexagonal structure in $BaNiO_3$ by changing the thickness of the sample and defocusing values in the imaging condition. A structure model and framework of unit cell are also shown. The defocusing values are represented with underfocus.

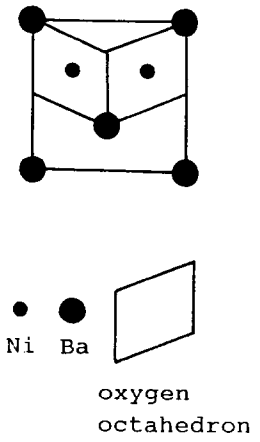

FIG. 7. Atomic arrangement of $BaNiO_3$ projected along the [100] direction of the hexagonal cell (*3*).

TABLE I

LATTICE DISTANCES AND RELATIVE INTENSITIES MEASURED BY X-RAY POWDER DIFFRACTION PATTERN OF FIG. 8 AND THE DATA FROM LANDER FOR THE PHASE WITH COMPOSITION NEAR $Ba_3Ni_3O_8$

d_{obs} (nm)	Intensity	*hkl*	d_{obs} (nm)[a]	Intensity[b]	*hkl*
0.34	S	320			
0.33	S	500	0.325	4	101
0.28	S	203	0.286	10	110
0.27	M	322			
0.24	W	132	0.25	1	200
0.22	S	220	0.22	7	201, 002
0.21	M	141			
0.20	W	233			
0.196	M	341	0.197	0.5	102
0.191	W	242	0.187	0.5	120
0.18	W	342			
0.17	M	250	0.172	7	121, 112

[a] From J. J. Lander (*3*).
[b] Maximum is 10.

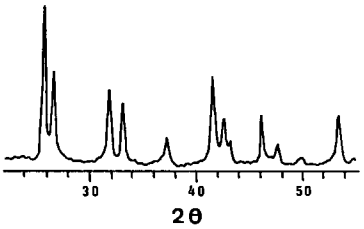

FIG. 8. X-ray powder diffraction pattern of an intermediate phase represented by the formula $BaNiO_x$ ($2 < x < 3$).

terns from the small areas indicated by B, C, and D, respectively, in Fig. 9a. Figures 9b and 9c were found to have the incident beam along the [100] direction in $BaNiO_3$ phase (mark B) and the [110] direction in $BaNiO_2$ phase (mark C), respectively. Figure 9d is from the intermediate region (mark D), which could give the relations of crystal orientation between $BaNiO_3$ and $BaNiO_2$. By analyzing the diffraction patterns, it could be concluded that the following topotaxial relations exist between $BaNiO_3$ and $BaNiO_2$: $[001]_{BaNiO_3}/[001]_{BaNiO_2}$ and $[100]_{BaNiO_3}/[1\bar{1}0]_{BaNiO_2}$.

Figures 10a and 10b show the low magnification and corresponding lattice image of $BaNiO_x$ crystals in the form of needlelike

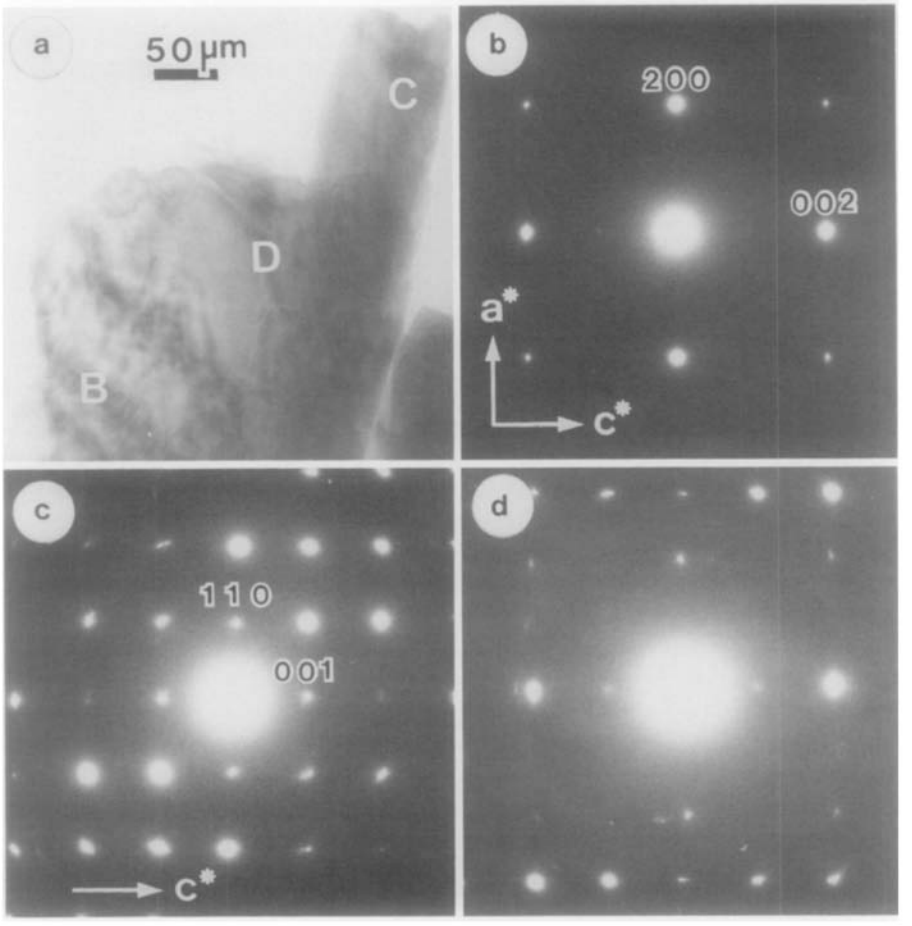

FIG. 9. Electron microscope image and diffraction patterns showing the topotaxial relation between $BaNiO_2$ and $BaNiO_3$. Selected area diffraction patterns of (b), (c), and (d) are from the regions B, C, and D marked in the image (a), respectively. B: $BaNiO_2$; C: $BaNiO_3$; and D: $BaNiO_x$ phases.

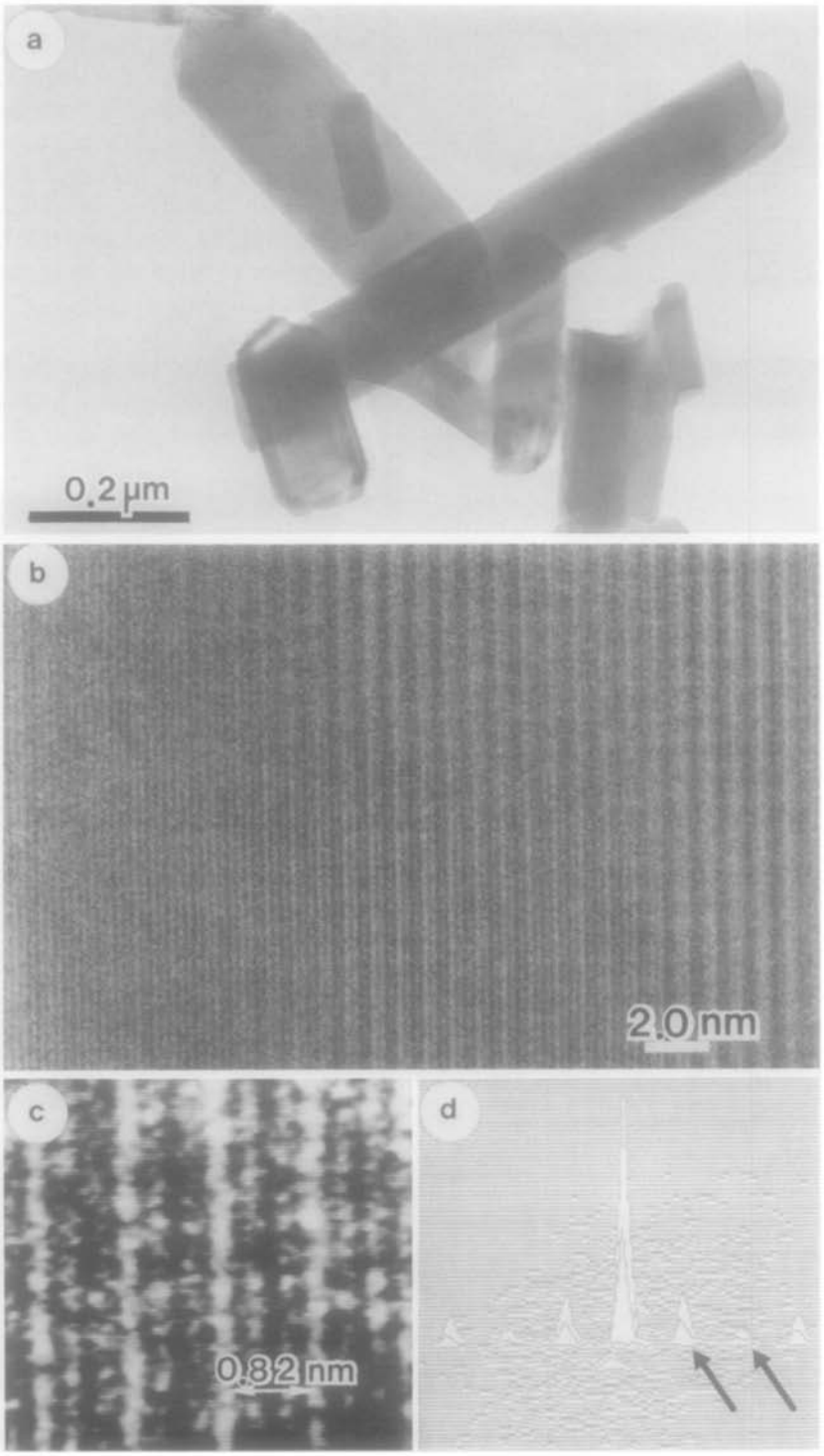

FIG. 10. Low-magnification and (b) lattice images of $BaNiO_x$ with incident beam parallel to the c-axis direction. Part (c) is an enlargement of (b) showing the lattice spacing of three times the spacing of the (100) plane in $BaNiO_2$ and (d) is a Fourier-transformed pattern of lattice image (b).

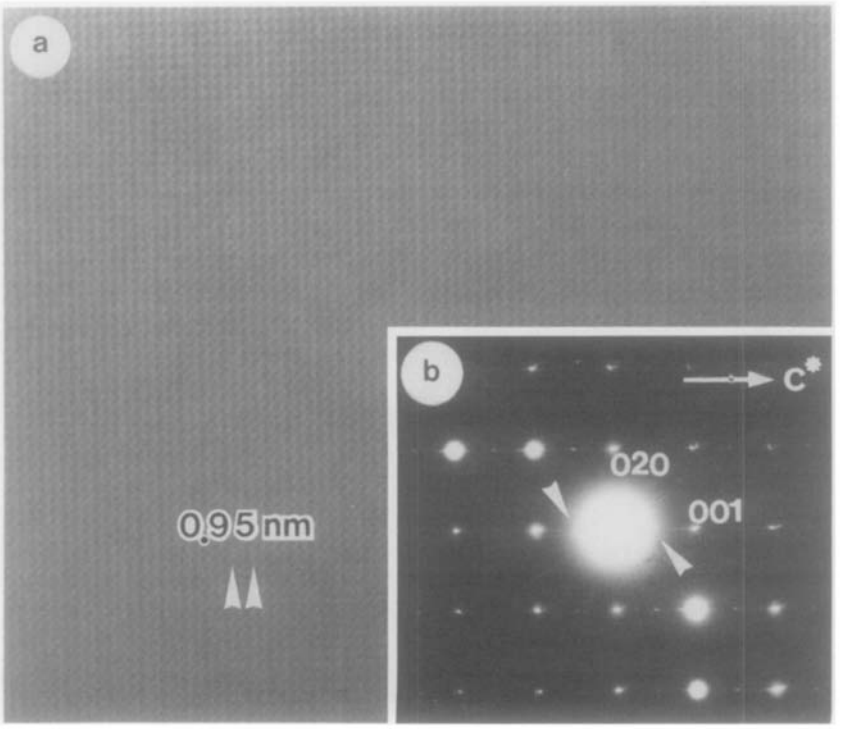

FIG. 11. (a) High-resolution image and (b) corresponding diffraction pattern of $BaNiO_x$ intermediate phase. Incident beam is parallel to the [100] direction in terms of an orthorhombic cell of $BaNiO_2$. The superlattice, which is about two times the spacing of the (001) plane in $BaNiO_2$ or $BaNiO_3$, is observed.

shapes, respectively, which is identical with that of Fig. 8. Figures 10c and 10d represent the enlargement and Fourier-transformed pattern of Fig. 10b, respectively. It was taken with an incident electron beam parallel to the [001] direction which is common to a hexagonal cell of $BaNiO_3$ and an orthorhombic cell of $BaNiO_2$. In Fig. 10c, fringes with a spacing of about 0.82 nm corresponding to three times the spacing of the (100) plane in a $BaNiO_2$ phase were observed. This scheme could also be confirmed by the pattern of Fig. 10d, which represents some diffraction spots due to a superlattice as indicated by the arrows.

Figures 11a and 11b also show the lattice image and corresponding diffraction pattern taken with an incidence parallel to the [100] direction in terms of an orthorhombic cell of $BaNiO_2$. A superstructure with lattice spacing of about 0.95 nm, which corresponds to about two times the spacing of the (001) plane in $BaNiO_2$ or $BaNiO_3$, was observed in the image and detected in the diffraction pattern as indicated by the arrows in (a) and (b). From the topotaxial relations deduced from Fig. 9 and the existence of the superlattice observed in Figs. 10 and 11, a new phase with the composition of $BaNiO_x$ ($2 < x < 3$) could have an orthorhombic cell represented by a superlattice of $BaNiO_2$ with $a_0 = 3a$, $b_0 = b$, $c_0 = 2c$ or of $BaNiO_3$ with $a_0 = 3a$, $c_0 = 2c$. Namely, the structure of the new phase has the unit cell parameter of $a = 1.63$, $b = 0.87$, $c = 0.89$ nm and a 1.48-nm^3 volume.

In order to confirm such a phase relation and structure of the new phase found in Ba

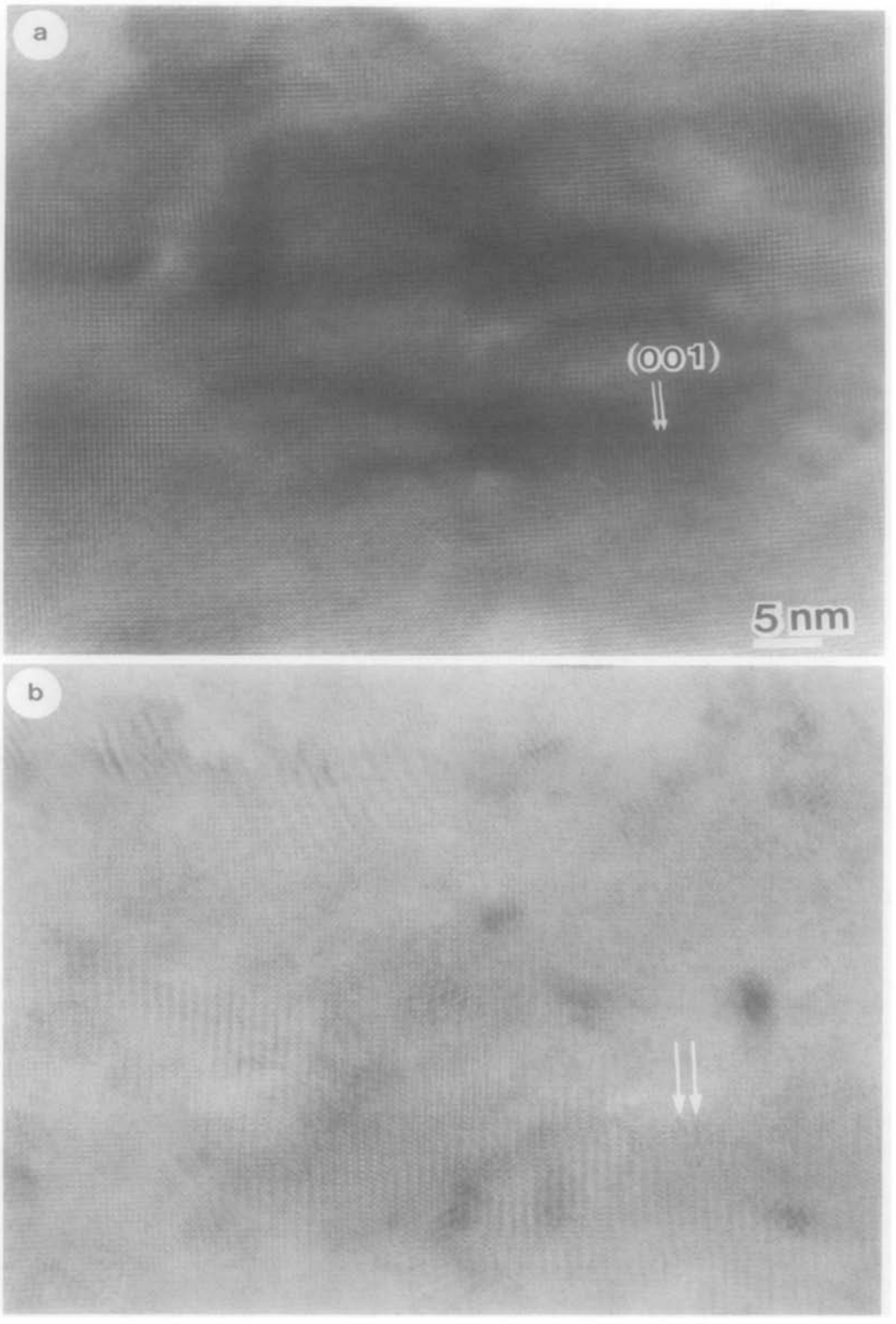

FIG. 12. High-resolution electron microscope image of transformation of $BaNiO_3$ phase into an intermediate phase of $BaNiO_x$ by beam irradiation in electron microscopy. (a) Initial stage and (b) final stage.

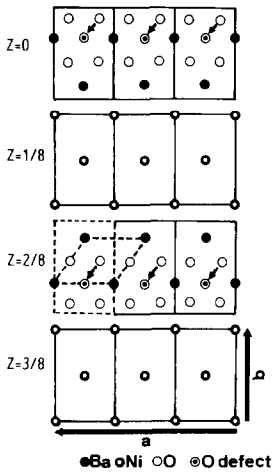

FIG. 13. Structure model of an intermediate phase showing half of the whole along the c-axis.

NiO_x, the process of transforming $BaNiO_3$ crystals into $BaNiO_x$ with nonstoichiometric state during beam irradiation was observed directly using electron microscopy. By irradiation of the sample consisting of the $BaNiO_3$ phase with a strong electron beam for about 20 min, a phase transformation took place, which is illustrated in Figs. 12a and 12b, which show the images at the initial and final stages of irradiation, respectively. Figure 12a shows the structure image of $BaNiO_3$ projected onto the $(1\bar{2}0)$ plane, which is identical to that of Fig. 5. The array of white dots corresponding to the spacing of (001) planes appeared in the image of Fig. 12a. But in Fig. 12b, image contrast with a long periodicity of twice the spacing of the (001) plane in $BaNiO_3$ was detected as indicated by the arrows. This fact could support the result of the formation of the superlattice as found in Figs. 10 and 11.

Figure 13 shows the structure model of a new phase deduced from a series of observations of the $BaNiO_x$ crystals illustrated in Figs. 9–12 and describes half of the unit cell projected along the c-axis. To indicate the phase relation between $BaNiO_2$ and $BaNiO_3$ clearly, the frameworks of their unit cells are drawn with dashed lines in the model. As mentioned above, the gross structure, especially with regard to the positions of Ba and Ni atoms, resembles those of $BaNiO_2$ and $BaNiO_3$. Therefore the formation of the superstructure in an intermediate phase could have its origin in the periodical defects of oxygen atoms assigned to an arrangement around nickel. From the periodicity of superstructure along the a- and c-axis as shown in Fig. 13, it could be considered that the compounds of $BaNiO_x$ with composition ranging between $BaNiO_{2.33}$ and $BaNiO_{2.67}$ had been formed. The positions of oxygen atoms which have the possibility of being reduced are marked by arrows in the model. Further adjustment, however, of coordinates of oxygen deficiency could not be attempted by means of X-ray powder diffraction or electron microscopy.

Acknowledgments

The author expresses deep gratitude to Professor H. Hashimoto for valuable discussions and thanks Mrs. B. Stein for correcting the manuscript. This work has been financially supported in part by the Kazato Foundation.

References

1. T. NEGAS AND R. S. ROTH, *J. Solid State Chem.* **3,** 323 (1971).
2. Y. SYONO, S. AKIMOTO, AND K. KOHN, *J. Phys. Soc. Japan.* **26,** 993 (1969).
3. J. J. LANDER, *Acta Crystallogr.* **4,** 148 (1951).
4. J. J. LANDER, *J. Amer. Chem. Soc.* **73,** 2450 (1950).
5. J. J. LANDER AND L. A. WOOTEN, *J. Amer. Chem. Soc.* **73,** 2452 (1950).
6. H. KRISCHNER, K. TORKAR, AND B. O. KOLBESEN, *J. Solid State Chem.* **3,** 349 (1971).
7. R. D. BURBANK AND H. T. EVANS, *Acta Crystallogr.* **1,** 330 (1948).
8. A. HARDY, *Acta Crystallogr., Sect. B* **15,** 179 (1962).

9. B. L. CHAMBERLAND, A. W. SLEIGHT, AND J. F. WEIHER, *J. Solid State Chem.* **1,** 506 (1970).
10. P. C. DONOHUE, L. KATZ, AND R. WARD, *Inorg. Chem.* **5,** No. 3, 339 (1966).
11. J. M. LONGO AND J. A. KAFALAS, *Mater. Res. Bull.* **3,** 687 (1968).
12. H. SHIBAHARA AND H. HASHIMOTO, *in* "Proceedings, 7th International Conference on Crystal Growth, Stuttgart"; *J. Cryst. Growth* **65,** 683 (1983).
13. H. SHIBAHARA, *J. Solid State Chem.* **66,** 116 (1987).
14. G. MALMROS AND J. O. THOMAS, *J. Appl. Crystallogr.* **10,** 7 (1977).
15. A. ALBINATI AND B. T. M. WILLIS, *J. Appl. Crystallogr.* **15,** 361 (1982).
16. J. M. COWELY AND A. F. MOODIE, *Acta Crystallogr.* **10,** 609 (1957).
17. P. GOODMAN AND A. F. MOODIE, *Acta Crystallogr., Sect. A* **30,** 280 (1974).